Exploring the Implications of 2023 Pular Timing Array Datasets for Scalar-Induced Gravitational Waves and Primordial Black Holes

Sai Wang,[1,2] Zhi-Chao Zhao,[3,*] Jun-Peng Li,[1,2] and Qing-Hua Zhu[4]

[1] *Theoretical Physics Division, Institute of High Energy Physics, Chinese Academy of Sciences, Beijing 100049, People's Republic of China*

[2] *School of Physical Sciences, University of Chinese Academy of Sciences, Beijing 100049, People's Republic of China*

[3] *Department of Applied Physics, College of Science, China Agricultural University, Qinghua East Road, Beijing 100083, People's Republic of China*

[4] *CAS Key Laboratory of Theoretical Physics, Institute of Theoretical Physics, Chinese Academy of Sciences, Beijing 100190, People's Republic of China*

Significant evidence for a gravitational-wave background was reported by several pulsar-timing-array collaborations. By assuming that this signal is interpreted by the scalar-induced gravitational waves, we study physical implications of the observed signal for the nature of primordial curvature perturbations and primordial black holes. In particular, we explore the effects of primordial non-Gaussianity on the inferences of model parameters, and obtain the parameter region allowed by the observed signal, i.e., the primordial scalar spectral amplitude $A_S \sim 10^{-2} - 1$, the primordial non-Gaussian parameter $-10 \lesssim f_{\rm NL} \lesssim 10$, and the mass of primordial black holes $m_{\rm pbh} \sim 10^{-3} - 0.1 M_{\odot}$. We find that the non-Gaussianity suppressing the abundance of primordial black holes is preferred by the observed signal. We show that the anisotropies of scalar-induced gravitational waves are a powerful probe for measurements of the non-Gaussian parameter $f_{\rm NL}$, and conduct a complete analysis of the angular power spectrum in the nano-Hertz band. We expect that the Square Kilometre Array project has potentials to measure such anisotropies.

I. INTRODUCTION

Recently, several observational collaborations of pulsar timing array (PTA) reported significant evidence for an excess signal with Hellings-Downs (HD) correlations [1–4], indicating the gravitational-wave origin of this signal. The strain amplitude of such a gravitational-wave background (GWB) was found to be of order 10^{-15} at the pivot frequency 1 yr^{-1}. The inferred GWB

* Corresponding author: zhaozc@cau.edu.cn

spectrum was found to be consistent with the astrophysical origin due to inspiraling supper-massive black hole (SMBH) binaries [5]. However, the current datasets could not exclude possibilities of cosmological origins (and other exotic astrophysical sources), which were studied by the collaborations in several accompany papers [6, 7]. In particular, many models of cosmological origins have been shown to provide even better fits to the observed signal than the SMBH-binary interpretation. If confirmed in future, they may point to evidence for new physics.

In this work, we will focus on the cosmological interpretation to the observed signal, i.e., the scalar-induced gravitational waves (SIGWs) [8–13]. This possibility was previously considered to account for the NANOGrav 12.5-year dataset [14] by the authors of Refs. [15–24]. Recently, it was revisited by the collaborations in Refs. [6, 7], but only the Gaussian primordial scalar (or equivalently, comoving curvature) perturbations were considered in the above studies. However, it has been shown that the primordial non-Gaussianity contributes a lot to the energy density of SIGWs [25–33], indicating significant modifications to the energy-density fraction spectrum that is essential for the data analysis of PTA observations. By interpreting the observed signal to have a SIGW origin, therefore, we will study implications of the PTA datasets for the nature of primordial scalar perturbations, including the power spectrum and the local-type primordial scalar non-Gaussianity.

We will also study physical implications for scenarios of primordial black holes (PBHs). The formation process of PBHs was accompanied by the inevitable production of SIGWs. In fact, the enhanced curvature perturbations not only produced PBHs due to gravitational collapse in the early universe [34], but also induced a GWB via nonlinear mode-couplings. Therefore, we can explore the PBH scenario by using SIGWs [35–38]. Related works analyzing realistic datasets can be found in Refs. [6, 7, 20–22, 38, 39]. Some strong influences of primordial non-Gaussianity on the mass function of PBHs were also studied in literature [24, 40–52]. In this work, by taking into account the effects of primordial non-Gaussianity, we will recast the constraints on primordial perturbations into the constraints on the mass function of PBHs [1].

To further explore the primordial non-Gaussiantiy, we will study the anisotropies in SIGWs in the PTA band and provide a complete analysis for the angular power spectrum in the same band. It was known that the energy-density spectrum of isotropic SIGWs has significant degeneracies of

[1] Note added: At the time of writing the current paper, there appeared a related paper [53] that analyzed the posteriors of NANOGrav 15-year (NG15) data. The authors claimed that the Gaussian scenarios for SIGWs are in tension with the current PTA data at 2σ confidence level, but the non-Gaussian scenarios that suppress the abundance of PBHs can alleviate such a tension. Due to large uncertainties in formation scenarios of PBHs (e.g., see reviews in Ref. [54]), one of the leading aims for our current work is a comprehensive study on the primordial non-Gaussianity. Full Bayesian analysis taking into the effects of primordial non-Gaussianity on SIGWs will be left to our future works.

model parameters [33]. Conducting a complete analysis of angular power spectrum, we showed that the angular power spectrum is useful for determining f_{NL}, because the above degeneracies would be broken if the anisotropic SIGWs are considered [33]. Earlier related works can be found in Refs. [54–62]. In this work, in the PTA band, we will further study the angular power spectrum for the anisotropies in SIGWs, which may be not only useful for determining f_{NL}, but also important for discriminating different GWB sources in realistic data analysis.

The remaining context of this paper is arranged as follows. In Section II, we will provide a brief summary of the isotropic SIGWs. In Section III, we will show implications of the current datasets for the power spectrum of primordial curvature perturbations and then for the mass function of PBHs. In Section IV, we will study the anisotropies in SIGWs and show the angular power spectrum in PTA band. In Section V, we make concluding remarks.

II. ENERGY-DENSITY FRACTION SPECTRUM OF SCALAR-INDUCED GRAVITATIONAL WAVES

In this section, we show a brief but self-consistent summary of the main results of SIGW theory.

The energy-density fraction spectrum of the isotropic GWB is $\bar{\Omega}_{\mathrm{gw}}(\eta, q) = \bar{\rho}_{\mathrm{gw}}(\eta, q)/\rho_{\mathrm{crit}}(\eta)$ [63], where q is the wavenumber of gravitational waves (GWs), ρ_{crit} is the critical energy density of the universe at the conformal time η, and the overbar denotes physical quantities of background level. The above definition indicates that $\int \bar{\rho}_{\mathrm{gw}}(\eta, q) \mathrm{d} \ln q$ is the total energy-density fraction of GWB [63]. The spectrum is formally expressed as $\bar{\rho}_{\mathrm{gw}}(\eta, q) \sim \langle h_{ij,l} h_{ij,l} \rangle$, where $h_{ij}(\eta, \mathbf{q})$ denotes the strain with wavevector $\mathbf{q}$ in Fourier space and the angle brackets define an ensemble average. For SIGWs on subhorizon scales, we have $h_{ij} \sim \zeta^2$ and then $\bar{\Omega}_{\mathrm{gw}}(\eta, \mathbf{q}) \sim \langle \zeta^4 \rangle$ [8, 9], where $\zeta(\mathbf{q})$ denotes the primordial curvature perturbations in the early universe. In the case of primordial Gaussianity, the semi-analytic formula for $\bar{\Omega}_{\mathrm{gw}}(\eta, \mathbf{q})$ was shown in Refs. [12, 13] and earlier related works can be found in Refs. [8, 9]. However, in the case of primordial non-Gaussianity, there is not such a semi-analytic formula. Related studies can be found in recent literature [25–33, 64]. In this work, we will follow the conventions of our previous work [33].

To derive the contributions of primordial non-Gaussianity to the energy density, we express the primordial curvature perturbations ζ in terms of their Gaussian components ζ_g, i.e., [65]

$$\zeta(\mathbf{q}) = \zeta_g(\mathbf{q}) + \frac{3}{5} f_{\mathrm{NL}} \int \frac{\mathrm{d}^3 \mathbf{k}}{(2\pi)^{3/2}} \zeta_g(\mathbf{k}) \zeta_g(\mathbf{q} - \mathbf{k}) \ , \tag{1}$$

where f_{NL} is the non-linear parameter characterizing the local-type primordial non-Gaussianity. We introduce a new quantity of $F_{\mathrm{NL}} = 3 f_{\mathrm{NL}}/5$ that will simplifies the analytic formulae in the

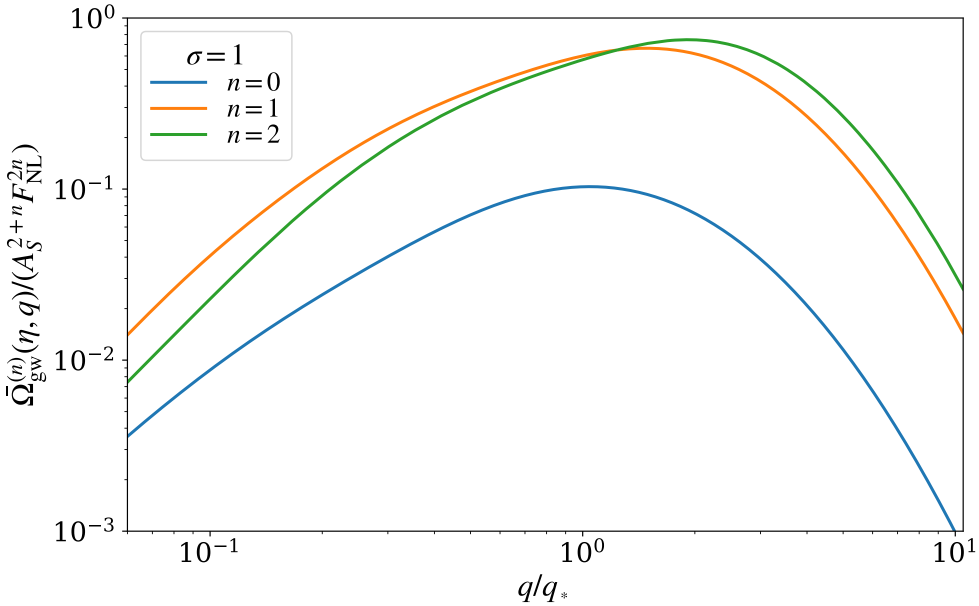

FIG. 1. Unscaled (or equivalently, $A_S = 1$ and $F_{\rm NL} = 1$) contributions to the energy-density fraction spectrum of isotropic SIGWs. We produce this figure by using the original data of Ref. [33].

following. Note that the validation of perturbation theory requires $A_S F_{\rm NL}^2 < 1$, where A_S will be defined in the following. We define the dimensionless power spectrum of ζ_g as follows

$$\langle \zeta_g(\mathbf{q}) \zeta_g(\mathbf{q}') \rangle = \delta^{(3)}(\mathbf{q} + \mathbf{q}') \frac{2\pi^2}{q^3} \Delta_g^2(q) \ , \tag{2}$$

where $\Delta_g^2(q)$ is assumed to be a normal function with respect to $\ln q$ in this work, i.e., [21, 31, 66, 67]

$$\Delta_g^2(q) = \frac{A_S}{\sqrt{2\pi\sigma^2}} \exp\left(-\frac{\ln^2(q/q_*)}{2\sigma^2} \right) \ . \tag{3}$$

Here, A_S stands for the spectral amplitude at the spectral peak wavenumber q_*, and σ denotes the standard deviation characterizing the width of spectrum. The wavenumber q can be straightforwardly recast into the frequency ν, namely, $q = 2\pi\nu$ and $q_* = 2\pi\nu_*$.

By conducting a tedious but straightforward derivation process, we can decompose $\bar{\Omega}_{\rm gw} \sim \langle \zeta^4 \rangle$ into three components depending on the power of $f_{\rm NL}$, based on the Wick's theorem. However, the complete derivations have been simplified by following an approach of Feynman-like diagrams [25, 28, 30–33]. We summarize only the final results as follows

$$\bar{\Omega}_{\rm gw}(\eta, q) = \bar{\Omega}_{\rm gw}^{(0)}(\eta, q) + \bar{\Omega}_{\rm gw}^{(1)}(\eta, q) + \bar{\Omega}_{\rm gw}^{(2)}(\eta, q) \ , \tag{4}$$

where we show the analytic expressions of $\bar{\Omega}_{\rm gw}^{(n)} \propto A_S^2 (A_S F_{\rm NL}^2)^n$ explicitly in Appendix A. They have been computed with the `vegas` package [68], and the numerical results are reproduced in

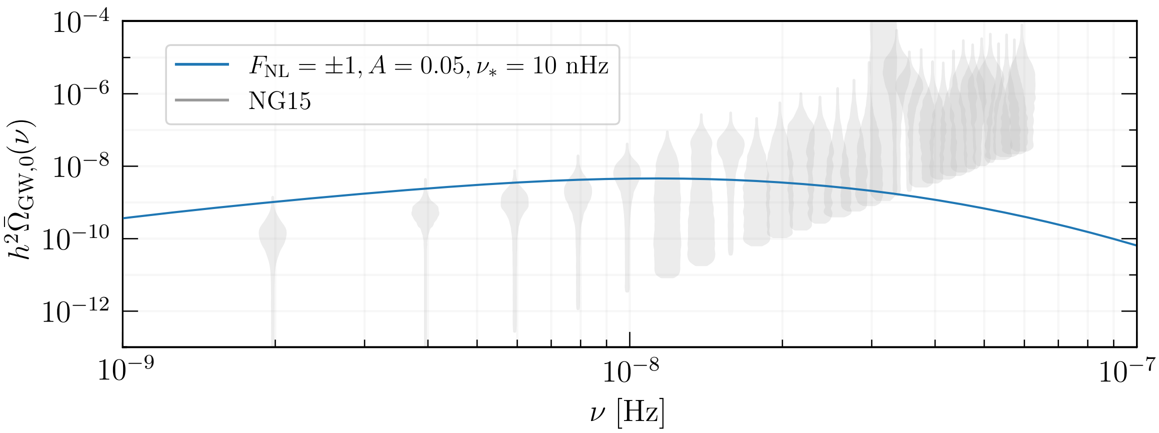

FIG. 2. Energy-density fraction spectrum of isotropic SIGWs. The NANOGrav 15-year data points [7] are shown for comparison. Here, we fix $\sigma = 1$.

Fig. 1. In particular, $\bar{\Omega}_{\mathrm{gw}}^{(0)}$ is exactly the result of energy-density fraction spectrum corresponding to the case of primordial Gaussianity, while $\bar{\Omega}_{\mathrm{gw}}^{(1)}$ and $\bar{\Omega}_{\mathrm{gw}}^{(2)}$ completely describe the contributions of local-type primordial non-Gaussianity.

The energy-density fraction spectrum of SIGWs at the current conformal time η_0 is given by

$$\bar{\Omega}_{\mathrm{gw},0}(\nu) \; = \; \Omega_{\mathrm{rad},0} \left(\frac{g_{*,\rho}(T)}{g_{*,\rho}(T_{\mathrm{eq}})} \right) \left(\frac{g_{*,s}(T_{\mathrm{eq}})}{g_{*,s}(T)} \right)^{4/3} \bar{\Omega}_{\mathrm{gw}}(\eta, q) \; , \tag{5}$$

where $\Omega_{\mathrm{rad},0} h^2 = 4.2 \times 10^{-5}$ is the physical energy-density fraction of radiations in the present universe [69], T (and T_{eq}) labels the cosmic temperatures at the emission time (and the epoch of matter-radiation equality), and ν denotes the gravitational-wave frequency, i.e., [21]

$$\frac{\nu}{\mathrm{nHz}} = 26.5 \left(\frac{T}{\mathrm{GeV}} \right) \left(\frac{g_{*,\rho}(T)}{106.75} \right)^{1/2} \left(\frac{g_{*,s}(T)}{106.75} \right)^{-1/3} \; . \tag{6}$$

Here, the effective relativistic degrees of the universe, i.e., $g_{*,\rho}$ and $g_{*,s}$, are tabulated functions of T, as shown in Ref. [70]. To illustrate the SIGW-interpretation of the current datasets, we depict $\bar{\Omega}_{\mathrm{gw},0}(\nu)$ as a function of ν in Fig. 2, by choosing a particular set of model parameters.

III. IMPLICATIONS OF PTA DATASETS FOR PRIMORDIAL CURVATURE PERTURBATIONS AND PRIMORDIAL BLACK HOLES

In this section, we study possible constraints on the parameter space of primordial power spectrum and PBHs from the NG15 data. Constraints from other PTA datasets can also be obtained following the same approach, but disregarded in this work.

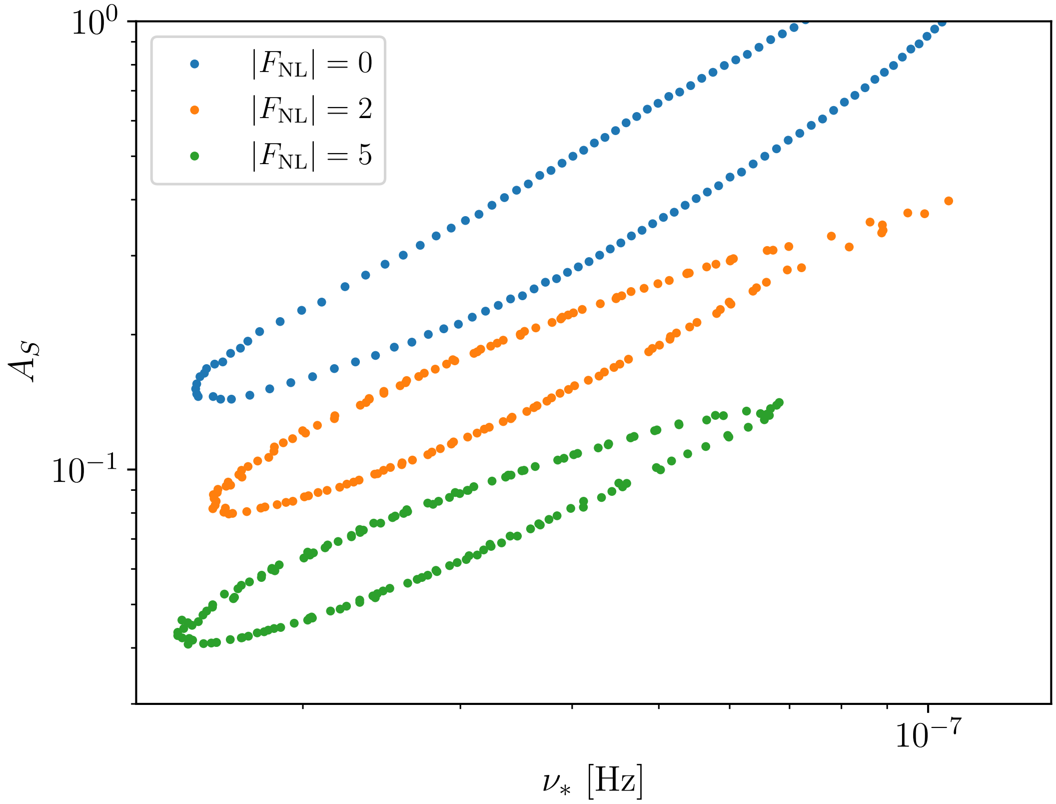

FIG. 3. Contours of the 68% probability regions for the spectral amplitude A_S and peak frequency ν_* defined in Eq. (3). Different values of $|F_{\rm NL}|$ have been considered, but σ is fixed to unity.

A. Primordial curvature perturbations

Based on the principle of PTA observations, the energy density of a given GWB, denoted with $\Omega_{\rm gw}(\nu)$ here, is related with the timing residual power spectral density $S(\nu)$, i.e., [7]

$$\Omega_{\rm gw}(\nu) = \frac{8\pi^4 \nu_{\rm yr}^5}{H_0^2} \left(\frac{\nu}{\nu_{\rm yr}}\right)^5 S(\nu) \ , \tag{7}$$

where $\nu_{\rm yr}$ is a pivot frequency related to a duration time of one year. For the realistic data analysis, $S(\nu)$ could be assumed to be power-law, i.e., [7]

$$S(\nu) = \frac{A^2}{12\pi^2} \left(\frac{\nu}{\nu_{\rm yr}}\right)^{-\gamma} {\rm yr}^3 \ , \tag{8}$$

where the amplitude A and index γ have been constrained by the NG15 data. For example, based on Fig. 1 of Ref. [7], the green contours in $\log_{10} A - \gamma$ plane stand for 68% (inner) and 95% (outer) probability regions.

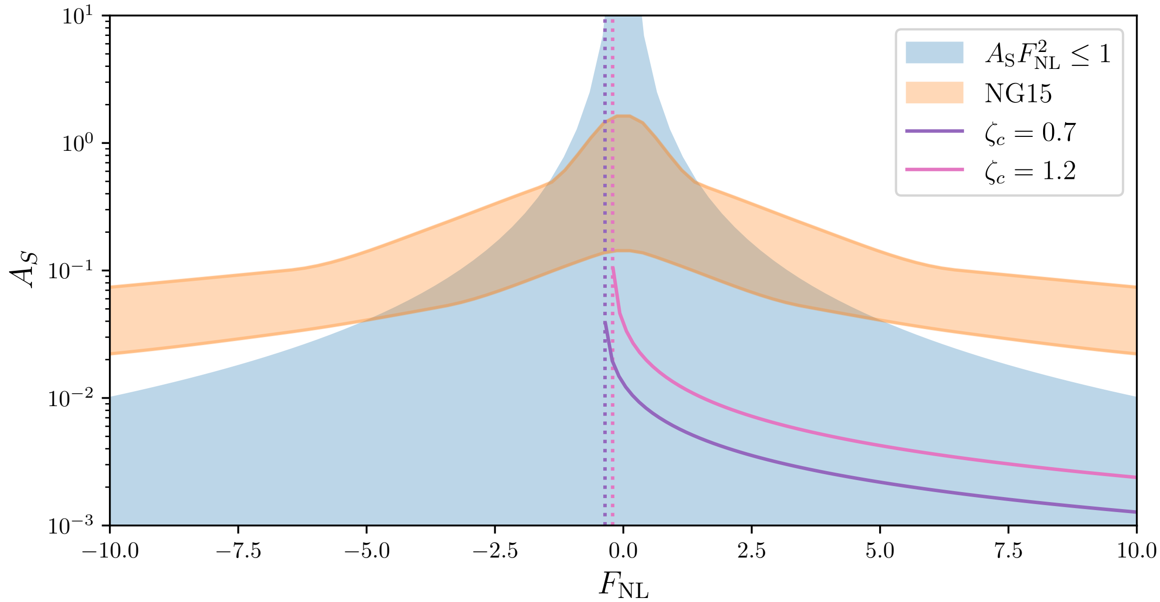

FIG. 4. Validation of perturbation theory versus the inferred parameter region (68% confidence level) from the NG15 data. The dotted lines denote $F_{\rm NL} = -(4\zeta_c)^{-1}$ and the solid curves denote $m_{\rm pbh} = 10^{-2}M_\odot$ and $f_{\rm pbh} = 1$ in the case of $\zeta_c = 0.7$ (purple color) and $\zeta_c = 1.2$ (rose color).

Though a full Bayesian analysis is of necessity in the future, we can immediately get some useful insights by recasting the contours in $\log_{10} A - \gamma$ plane into the contours in $A_S - \nu_*$ plane, once σ and $|F_{\rm NL}|$ take definitive values. Fig. 3 displays such contours for a series of values of $|F_{\rm NL}|$, denoted with colored dots. Hereafter, we fix the value of σ, namely, $\sigma = 1$, but a generalization is straightforward. In fact, such a choice is consistent with the best-fit σ from the NG15 data, which resulted in a 68% credible interval $\sigma \in [0.51, 2.07]$ [7]. To conduct such recasting manipulations, for a given set of A and γ, we should vary A_S and ν_* to make $\bar{\Omega}_{\rm gw,0}(\nu)$ following the same power-law as $\Omega_{\rm gw}(\nu)$. Here, we have fixed the pivot scale to be $\nu_{\rm yr}$ for the model parameters A_S and ν_*. The above approach was already adopted in literature [17].

Based on Fig. 3, we find significant effects of non-Gaussian parameter $|F_{\rm NL}|$ on the inferences of other parameters A_S and ν_*, and vice versa. In particular, the contours are shifted to lower-A_S regimes with the increase of $|F_{\rm NL}|$, since the energy density of SIGWs would be overproduced in the presence of primordial non-Gaussianity. This is one of the important results of this work. Though our research method can be straightforwardly generalized to other values of σ, it is essential to conduct a full Bayesian analysis that is left to our future works. Note that the above results are independent of the non-Gaussian sign. However, the non-Gaussian sign would significantly affect the mass function of PBHs that will be studied in the following.

We further pin down the parameter region of A_S and $F_{\rm NL}$, by considering the validation of perturbation theory that requires $A_S F_{\rm NL}^2 \leq 1$. In Fig. 4, the blue shaded area corresponds to such a requirement, while the orange shaded area corresponds to the inferred parameter region (68% confidence level) from the NG15 data. Only the overlap area is simultaneously allowed by theory and observations. In this sense, the PTA observations have already been a powerful probe of the early universe.

B. Primordial black holes

We further recast the constraints on the primordial curvature perturbations into the constraints on PBHs. Due to large uncertainties for the formation scenarios of PBHs (e.g., see reviews in Ref. [54]), we consider a simplified scenario used by Ref. [48] to demonstrate the importance of primordial non-Gaussianity. The initial mass function of PBHs is given by

$$\beta = \int_{\zeta>\zeta_c} P(\zeta) d\zeta = \int_{\zeta(\zeta_g)>\zeta_c} \frac{1}{\sqrt{2\pi}\sigma_g} \exp\left(-\frac{\zeta_g^2}{2\sigma_g^2}\right) d\zeta_g \ , \tag{9}$$

where $P(\zeta)$ is a probability distribution function (PDF) of primordial curvature perturbations, σ_g is a standard variance for a PDF of Gaussian component ζ_g, and ζ_c denotes the critical fluctuation. Considering the power spectrum in Eq. (3), we obtain $\sigma_g^2 = \langle \zeta_g^2 \rangle = \int \Delta_g^2(q) d\ln q = A_S$. In addition, it is known that $\zeta_c \sim \mathcal{O}(1)$, which was shown to be 0.7 and 1.2 in Ref. [71]. We will consider both of them in the following.

To calculate Eq. (9), we separate $F_{\rm NL}$ into two regimes, i.e., $F_{\rm NL} > 0$ and $F_{\rm NL} < 0$. As the first step, we solve the equation $\zeta(\zeta_g) = \zeta_c$ to get the following relation

$$\zeta_{g\pm} = \frac{-1 \pm \sqrt{1 + 4F_{\rm NL}\zeta_c}}{2F_{\rm NL}} \ . \tag{10}$$

By substituting it into Eq. (9), we have an expression of β for $F_{\rm NL} > 0$, i.e.,

$$\beta = \left(\int_{-\infty}^{\zeta_{g-}} + \int_{\zeta_{g+}}^{+\infty}\right) P(\zeta_g) d\zeta_g = \frac{1}{2}\mathrm{erfc}\left(\frac{\zeta_{g+}}{\sqrt{2A_S}}\right) + \frac{1}{2}\mathrm{erfc}\left(-\frac{\zeta_{g-}}{\sqrt{2A_S}}\right) \ , \tag{11}$$

where erfc(x) is the complementary error function. Similarly, for $-(4\zeta_c)^{-1} < F_{\rm NL} < 0$, we have

$$\beta = \int_{\zeta_{g+}}^{\zeta_{g-}} P(\zeta_g) d\zeta_g = \frac{1}{2}\mathrm{erfc}\left(\frac{\zeta_{g+}}{\sqrt{2A_S}}\right) - \frac{1}{2}\mathrm{erfc}\left(\frac{\zeta_{g-}}{\sqrt{2A_S}}\right) \ . \tag{12}$$

However, for $F_{\rm NL} < -(4\zeta_c)^{-1}$, no PBHs were formed in the early universe, because the curvature perturbations are expected to never exceed the critical fluctuation. As a reasonable candidate of cold dark matter, the abundance of PBHs is given as [72]

$$f_{\rm pbh} \simeq 2.5 \times 10^8 \beta \left(\frac{g_{*,\rho}(T_{\rm f})}{10.75}\right)^{-1/4} \left(\frac{m_{\rm pbh}}{M_\odot}\right)^{-1/2} \ . \tag{13}$$

where $m_{\rm pbh}$ stands for the mass of PBHs in units of $M_\odot$, and $T_{\rm f}$ denotes the cosmic temperature at the formation time. Roughly speaking, $m_{\rm pbh}$ can be related with the horizon mass m_H and then the frequency ν_*. To be specific, we have [17]

$$\frac{m_{\rm pbh}}{M_\odot} \simeq \frac{m_H}{0.31 M_\odot} \simeq \left(\frac{\nu_*}{5.0{\rm nHz}}\right)^{-2} . \tag{14}$$

Therefore, we infer the mass of PBHs to be $\sim \mathcal{O}(10^{-3} - 10^{-1})M_\odot$, based on Fig. 3. However, the inferred abundance would be larger than unity, indicating that the PBH scenario is in tension with the NG15 data. To demonstrate this result more clearly, in Fig. 4, we depict two solid curves corresponding to $m_{\rm pbh} = 10^{-2}M_\odot$ and $f_{\rm pbh} = 1$ in the case of $\zeta_c = 0.7$ (purple curve) and $\zeta_c = 1.2$ (rose curve). We also denote the critical value $F_{\rm NL} = -(4\zeta_c)^{-1}$ with vertical dotted lines.

Based on Fig. 4, when we interpret the observed signal to have a SIGW origin, we find overproduction of PBHs, since the inferred value of A_S is typically one order of magnitude larger than the value of A_S producing $f_{\rm pbh} = 1$. Even if we take into account the effects of positive non-Gaussianity, such overproduction can not be effectively alleviated. In contrast, the negative non-Gaussianity can alleviate it, particularly when we consider a sizable negative non-Gaussian parameter, i.e., $F_{\rm NL} < -(4\zeta_c)^{-1}$, that forbids any formation of PBHs. Due to large uncertainties, it is challenging to exclude the PBH scenario by analyzing the current datasets. However, a more-detailed analysis such as the Bayesian analysis is still important, but beyond the scope of the current paper.

Therefore, it seems essential to measure the primordial non-Gaussianity, at least determine the sign of $F_{\rm NL}$ in order to judge the PBH scenario. However, due to the sign degeneracy of $F_{\rm NL}$, it is impossible to determine the non-Gaussian sign via measurements of the energy-density fraction spectrum of SIGWs. In the next section, we will propose that the anisotropic SIGWs have potentials to break such a sign degeneracy as well as other degeneracies of model parameters, providing some possibilities for judgements of the PBH scenario in future.

IV. ANGULAR POWER SPECTRUM FOR ANISOTROPIES IN SCALAR-INDUCED GRAVITATIONAL WAVES

In this section, we study the anisotropies in SIGWs as well as the angular power spectrum in the PTA band, following the conventions of our previous paper [33].

The anisotropies in SIGWs arise from long-wavelength modulations of the energy density produced by short-wavelength modes. Based on Section II, we know that SIGW were produced at extremely high redshifts, corresponding to extremely small horizons. Due to limitation in the

angular resolution of gravitational-wave detectors, the signal along a line-of-sight stands for an ensemble average of the energy densities over a quantity of such horizons. In this sense, any two signals would be identical. However, the energy density of SIGWs that were produced by short-wavelength modes can be spatially redistributed by long-wavelength modes, if there are couplings between the short- and long-wavelength modes. Therefore, the primordial non-Gaussianity of local type could have contributions to such couplings, as shown in the following.

Analogue to the temperature fluctuations of relic photons [73], the initial inhomogeneities in SIGWs at spatial location $\mathbf{x}$ are characterized with the density contrast, i.e., $\delta_{\mathrm{gw}}(\eta,\mathbf{x},\mathbf{q}) = 4\pi\omega_{\mathrm{gw}}(\eta,\mathbf{x},\mathbf{q})/\bar{\Omega}_{\mathrm{gw}}(\eta,q) - 1$. Here, the energy-density full spectrum $\omega_{\mathrm{gw}}(\eta,\mathbf{x},\mathbf{q})$ is defined by the energy density $\rho_{\mathrm{gw}}(\eta,\mathbf{x}) = \rho_{\mathrm{crit}} \int \mathrm{d}^3\mathbf{q}\, \omega_{\mathrm{gw}}(\eta,\mathbf{x},\mathbf{q})/q^3$. This definition implies that we have $\omega_{\mathrm{gw}}(\eta,\mathbf{x},\mathbf{q}) \sim \langle\zeta^4\rangle_{\mathbf{x}}$, where the subscript $_{\mathbf{x}}$ stands for an ensemble average within the horizon enclosing $\mathbf{x}$ [33, 55]. We further separate ζ_g into short-wavelength ζ_{gS} and long-wavelength ζ_{gL}, i.e., $\zeta_g = \zeta_{gS} + \zeta_{gL}$ [74]. Finally, we obtain $\delta_{\mathrm{gw}}(\eta,\mathbf{x},\mathbf{q}) \sim \zeta_{gL}\langle\zeta_{gS}\zeta_S^3\rangle_{\mathbf{x}}$ at linear order of ζ_{gL}. Here, we introduce ζ_S to denote the part of ζ, which is composed of only ζ_{gS}. Higher orders of ζ_{gL} are negligible due to power spectrum $\Delta_L^2 \sim 10^{-9}$ for ζ_{gL} [69]. By using the Feynman-like rules and diagrams, we have obtained an explicit expression for $\delta_{\mathrm{gw}}(\eta,\mathbf{x},\mathbf{q})$ as follows [33]

$$\delta_{\mathrm{gw}}(\eta,\mathbf{x},\mathbf{q}) = \frac{3f_{\mathrm{NL}}}{5}\frac{\Omega_{\mathrm{ng}}(\eta,q)}{\bar{\Omega}_{\mathrm{gw}}(\eta,q)} \int \frac{d^3\mathbf{k}}{(2\pi)^{3/2}} e^{i\mathbf{k}\cdot\mathbf{x}} \zeta_{gL}(\mathbf{k}) \ , \tag{15}$$

where a new quantity is introduced for simplifying our computation, i.e.,

$$\Omega_{\mathrm{ng}}(\eta,q) = 2^3\bar{\Omega}_{\mathrm{gw}}^{(0)}(\eta,q) + 2^2\bar{\Omega}_{\mathrm{gw}}^{(1)}(\eta,q) \ . \tag{16}$$

The initial inhomogeneities here correspond to the intrinsic temperature fluctuations of cosmic microwave background (CMB) photons on the last-scattering surface.

The "observed" density contrast $\delta_{\mathrm{gw},0}(\mathbf{q})$ can be analytically estimated following the line-of-sight approach [75–77]. It is contributed by both of the initial inhomogeneities and some propagation effects, i.e, [33]

$$\delta_{\mathrm{gw},0}(\mathbf{q}) = \delta_{\mathrm{gw}}(\eta,\mathbf{x},\mathbf{q}) + \left[4 - n_{\mathrm{gw},0}(\nu)\right]\Phi(\eta,\mathbf{x}) \ , \tag{17}$$

where we consider only the Sachs-Wolfe (SW) effect [78], characterized by the Bardeen's potential at large scales, i.e.,

$$\Phi(\eta,\mathbf{x}) = \frac{3}{5}\int \frac{d^3\mathbf{k}}{(2\pi)^{3/2}} e^{i\mathbf{k}\cdot\mathbf{x}} \zeta_{gL}(\mathbf{k}) \ , \tag{18}$$

and $n_{\mathrm{gw},0}(\mathbf{q})$ is the index of the energy-density fraction spectrum defined in Eq. (5), i.e.,

$$n_{\mathrm{gw},0}(\nu) = \frac{\partial \ln \bar{\Omega}_{\mathrm{gw},0}(\nu)}{\partial \ln \nu} \simeq \frac{\partial \ln \bar{\Omega}_{\mathrm{gw}}(\eta,q)}{\partial \ln q}\Big|_{q=2\pi\nu} \ . \tag{19}$$

In the following, we adopt the assumption of statistical isotropy for the density contrasts on large scales. Analogue to the study of CMB (e.g., see Ref. [79]), the inhomogeneities in SIGWs can be recast into the anisotropies in GWB.

The reduced angular power spectrum is usually used for characterizing the statistics of the anisotropies in SIGWs. It is defined as the following two-point correlator

$$\langle \delta_{\mathrm{gw},0,\ell m}(2\pi\nu)\delta^{*}_{\mathrm{gw},0,\ell' m'}(2\pi\nu)\rangle = \delta_{\ell\ell'}\delta_{mm'}\widetilde{C}_{\ell}(\nu) \ , \tag{20}$$

where $\delta_{\mathrm{gw},0}(\mathbf{q})$ is expanded in terms of spherical harmonics, i.e., $\delta_{\mathrm{gw},0}(\mathbf{q}) = \sum_{\ell m} \delta_{\mathrm{gw},0,\ell m}(q) Y_{\ell m}(\mathbf{n})$. Roughly, we get $\tilde{C}_\ell \sim \delta^2_{\mathrm{gw},0} \propto \langle \zeta_{gL}\zeta_{gL}\rangle \sim \Delta^2_L$. A complete analysis employing the Feynman-like rules and diagrams has been conducted in our previous work [33]. We summarize only the final results as follows

$$\widetilde{C}_{\ell}(\nu) = \frac{18\pi\Delta_L^2}{25\ell(\ell+1)}\left[f_{\mathrm{NL}}\frac{\Omega_{\mathrm{ng}}(\eta,2\pi\nu)}{\bar{\Omega}_{\mathrm{gw}}(\eta,2\pi\nu)} + (4 - n_{\mathrm{gw},0}(\nu))\right]^2 \ , \tag{21}$$

which can be recast into the angular power spectrum, i.e.,

$$C_{\ell}(\nu) = \left(\frac{\bar{\Omega}_{\mathrm{gw},0}(\nu)}{4\pi}\right)^2 \tilde{C}_{\ell}(\nu) \ . \tag{22}$$

We make an analogue to the anisotropies in CMB, for which the rms temperature is roughly determined by $[\ell(\ell+1)C_\ell^{\mathrm{CMB}}/(2\pi)]^{1/2}$. For the anisotropies in SIGWs, the rms energy density is roughly determined by $[\ell(\ell+1)C_\ell(\nu)/(2\pi)]^{1/2}$, which is the variance of the energy-density fluctuations. Note that the rms energy density is constant with respect to the multipoles ℓ, but depends on the gravitational-wave frequency bands.

In Fig. 5, we depict the rms energy density with respect to the gravitational-wave frequency. For comparison, we also show the energy-density fraction spectrum in the same figure. Roughly speaking, we find $\sqrt{\tilde{C}_\ell} \sim \mathcal{O}(10^{-4})$, depending on the model parameters. Note that the angular power spectrum can break the degeneracies of model parameters. For example, based on Fig. 5, we find coincidence for the energy-density fraction spectra of three different sets of parameters. However, the angular power spectrum breaks such a coincidence, particularly, the sign degeneracy of F_{NL}. This result indicates that the primordial non-Gaussianity could be determined by measurements of the anisotropies in SIGWs in principle [33]. Recently, an upper limit on the reduced angular power spectrum was inferred to be $\tilde{C}_\ell < 20\%$ from the NG15 data [81]. It is not precise enough to test the theoretical predictions of our current work. In contrast, based on Fig. 5, we expect the Square Kilometre Array (SKA) [80] to have sufficient precision for measurements of the non-Gaussian parameter.

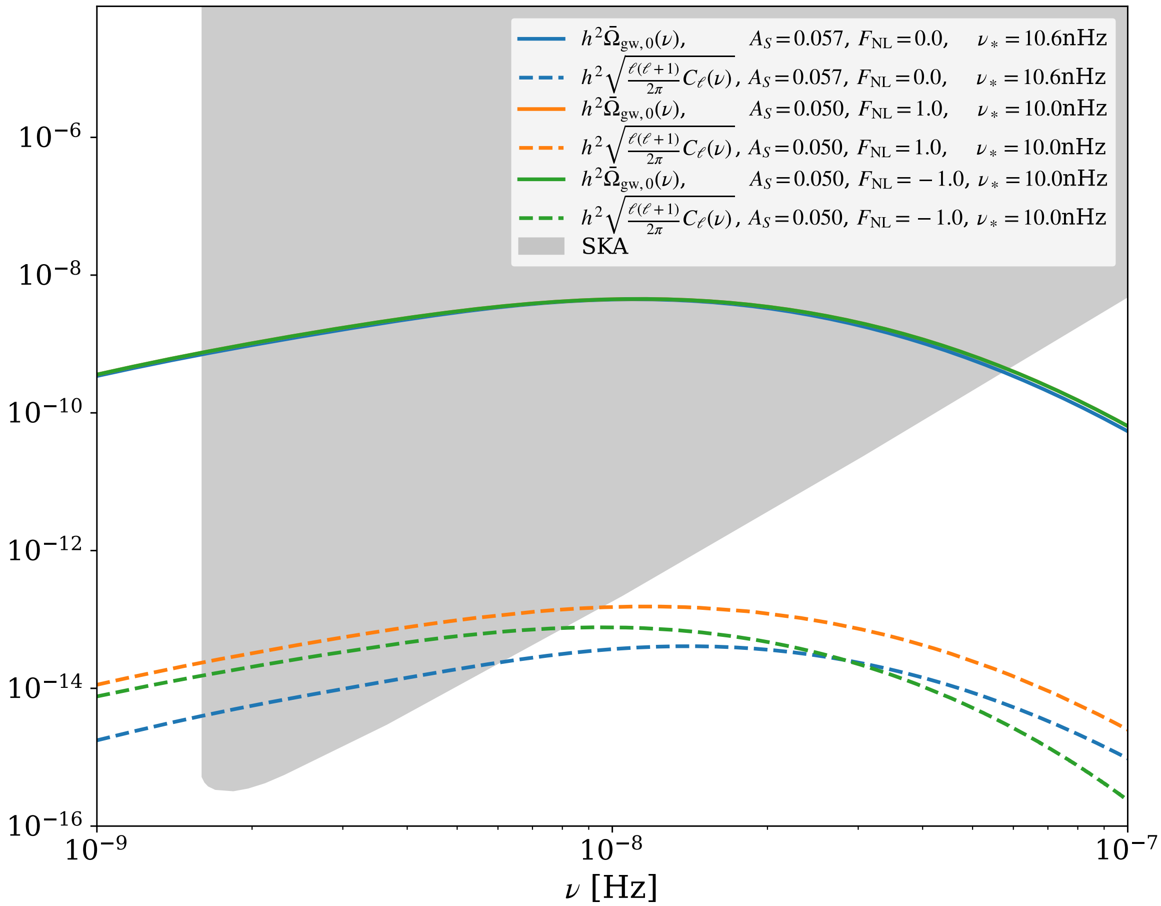

FIG. 5. Energy-density fraction spectra $h^2\Omega_{\mathrm{gw},0}(\nu)$ (solid curves) and the variance of energy-density anisotropies $h^2[\ell(\ell+1)C_\ell(\nu)/(2\pi)]^{1/2}$ (dashed curves) versus the sensitivity of Square Kilometre Array (SKA) [80] (gray shaded area).

V. CONCLUSIONS

In this work, we studied the implications of the recent PTA datasets for the nature of primordial curvature perturbations and primordial black holes. In particular, we explored the influence of primordial scalar non-Gaussianity on the inferences of model parameters, and vice versa. By taking into account the impacts of primordial non-Gaussianity, we analyzed the current datasets and obtained the allowed parameter region for the primordial scalar spectral amplitude $A_S \sim 10^{-2} - 1$, the primordial non-Gaussian parameter $-10 \lesssim F_{\rm NL} \lesssim 10$, and the mass of PBHs $m_{\rm pbh} \sim 10^{-2} - 1 M_\odot$. It is still important to stress the necessity of a full Bayesian analysis that will be conducted in the future. Even if the non-Gaussian parameter is considered, the PBH scenario was shown to be in tension with the NG15 data, except when we considered a sizable negative $F_{\rm NL}$ that can significantly suppress the abundance of PBHs. However, it is challenging to exclude the PBH scenario with

the current datasets, due to large uncertainties of formation models. Finally, we proposed that the anisotropies of SIGWs are a powerful probe for measurements of the non-Gaussian parameter F_{NL}, and conducted the first complete analysis of the angular power spectrum in the nano-Hertz band. In particular, we found that such a spectrum can effectively break some degeneracies of model parameters, particularly, the sign degeneracy of F_{NL}. In addition, we explored detectablity of the anisotropies in SIGWs in an era of the SKA project.

ACKNOWLEDGMENTS

S.W. and J.P.L. are supported by the National Natural Science Foundation of China (Grant NO. 12175243). Z.C.Z. is supported by the National Natural Science Foundation of China (Grant NO. 12005016).

Appendix A: Formulae for computing the SIGW energy density

After the lengthy and tedious derivation in accordance with Refs. [31–33], the three terms in Eq. (4) can be exactly expressed as follows

$$\bar{\Omega}_{\mathrm{gw}}^{(0)}(\eta,q) = \frac{1}{3}\int_0^\infty \mathrm{d}t_1 \int_{-1}^1 \mathrm{d}s_1\, \overbrace{J^2(u_1,v_1,x\to\infty)}\, \frac{1}{(u_1v_1)^2}\Delta_g^2(v_1q)\Delta_g^2(u_1q)\ , \tag{A1}$$

$$\begin{aligned}\bar{\Omega}_{\mathrm{gw}}^{(1)}(\eta,q) = \frac{F_{\mathrm{NL}}^2}{3\pi}\prod_{i=1}^{2}\left[\int_0^\infty \mathrm{d}t_i\int_{-1}^1\mathrm{d}s_i\, v_iu_i\right]&\left\{\frac{\pi\,\overbrace{J^2(u_1,v_1,x\to\infty)}}{(u_1v_1u_2v_2)^3}\Delta_g^2(v_1v_2q)\Delta_g^2(u_1q)\Delta_g^2(v_1u_2q)\right.\\ &+\int_0^{2\pi}\mathrm{d}\varphi_{12}\,\cos 2\varphi_{12}\,\overbrace{J(u_1,v_1,x\to\infty)J(u_2,v_2,x\to\infty)}\\ &\left.\times\frac{\Delta_g^2(v_2q)}{v_2^3}\frac{\Delta_g^2(w_{12}q)}{w_{12}^3}\left[\frac{\Delta_g^2(u_2q)}{u_2^3}+\frac{\Delta_g^2(u_1q)}{u_1^3}\right]\right\}\ ,\end{aligned} \tag{A2}$$

$$\begin{aligned}\bar{\Omega}_{\mathrm{gw}}^{(2)}(\eta,q) = \frac{F_{\mathrm{NL}}^4}{24\pi^2}\prod_{i=1}^{3}&\left[\int_0^\infty \mathrm{d}t_i\int_{-1}^1\mathrm{d}s_i\, v_iu_i\right]\\ &\left\{\frac{2\pi^2\,\overbrace{J^2(u_1,v_1,x\to\infty)}}{(u_1v_1u_2v_2u_3v_3)^3}\Delta_g^2(v_1v_2q)\Delta_g^2(v_1u_2q)\Delta_g^2(u_1v_3q)\Delta_g^2(u_1u_3q)\right.\\ &+\int_0^{2\pi}\mathrm{d}\varphi_{12}\mathrm{d}\varphi_{23}\,\cos 2\varphi_{12}\,\overbrace{J(u_1,v_1,x\to\infty)J(u_2,v_2,x\to\infty)}\\ &\left.\times\frac{\Delta_g^2(u_3q)}{u_3^3}\frac{\Delta_g^2(w_{13}q)}{w_{13}^3}\left[\frac{\Delta_g^2(v_3q)}{v_3^3}\frac{\Delta_g^2(w_{23}q)}{w_{23}^3}+\frac{\Delta_g^2(w_{23}q)}{w_{23}^3}\frac{\Delta_g^2(w_{123}q)}{w_{123}^3}\right]\right\}\ ,\end{aligned} \tag{A3}$$

where we define $x = q\eta$, $s_i = u_i - v_i$, $t_i = u_i + v_i - 1$, and

$$y_{ij} = \frac{\cos\varphi_{ij}}{4}\sqrt{t_i(t_i+2)(1-s_i^2)t_j(t_j+2)(1-s_j^2)} + \frac{1}{4}[1-s_i(t_i+1)][1-s_j(t_j+1)] \ , \tag{A4a}$$

$$w_{ij} = \sqrt{v_i^2 + v_j^2 - y_{ij}} \ , \tag{A4b}$$

$$w_{123} = \sqrt{v_1^2 + v_2^2 + v_3^2 + y_{12} - y_{13} - y_{23}} \ . \tag{A4c}$$

The oscillation average of squared $J(u, v, x \to \infty)$ has been given by Ref. [33] and the earlier works in Refs. [12, 13, 30, 31], i.e.,

$$\begin{aligned}
&\overbrace{J(u_i, v_i, x \to \infty) J(u_j, v_j, x \to \infty)} \\
&= \frac{9\left(1-s_i^2\right)\left(1-s_j^2\right) t_i\left(t_i+2\right) t_j\left(t_j+2\right)\left(s_i^2+t_i^2+2t_i-5\right)\left(s_j^2+t_j^2+2t_j-5\right)}{8\left(-s_i+t_i+1\right)^3\left(s_i+t_i+1\right)^3\left(-s_j+t_j+1\right)^3\left(s_j+t_j+1\right)^3} \\
&\quad \left[\left(\left(s_i^2+t_i^2+2t_i-5\right)\ln\left(\left|\frac{t_i^2+2t_i-2}{s_i^2-3}\right|\right)+2\left(s_i-t_i-1\right)\left(s_i+t_i+1\right)\right)\right. \\
&\quad\quad \left(\left(s_j^2+t_j^2+2t_j-5\right)\ln\left(\left|\frac{t_j^2+2t_j-2}{s_j^2-3}\right|\right)+2\left(s_j-t_j-1\right)\left(s_j+t_j+1\right)\right) \\
&\quad\quad \left.+\pi^2\Theta\left(t_i-\sqrt{3}+1\right)\Theta\left(t_j-\sqrt{3}+1\right)\left(s_i^2+t_i^2+2t_i-5\right)\left(s_j^2+t_j^2+2t_j-5\right)\right] .
\end{aligned} \tag{A5}$$

The formulae in this appendix can be used for numerically computing the energy density of SIGWs in a self-consistent way.

---

[1] H. Xu et al., *Searching for the Nano-Hertz Stochastic Gravitational Wave Background with the Chinese Pulsar Timing Array Data Release I*, Res. Astron. Astrophys. **23** (2023) 075024 [2306.16216].

[2] J. Antoniadis et al., *The second data release from the European Pulsar Timing Array III. Search for gravitational wave signals*, 2306.16214.

[3] NANOGrav collaboration, *The NANOGrav 15-year Data Set: Evidence for a Gravitational-Wave Background*, Astrophys. J. Lett. **951** (2023) [2306.16213].

[4] D.J. Reardon et al., *Search for an isotropic gravitational-wave background with the Parkes Pulsar Timing Array*, Astrophys. J. Lett. **951** (2023) [2306.16215].

[5] NANOGrav collaboration, *The NANOGrav 15-year Data Set: Constraints on Supermassive Black Hole Binaries from the Gravitational Wave Background*, 2306.16220.

[6] J. Antoniadis et al., *The second data release from the European Pulsar Timing Array: V. Implications for massive black holes, dark matter and the early Universe*, 2306.16227.

[7] NANOGrav collaboration, *The NANOGrav 15-year Data Set: Search for Signals from New Physics*, Astrophys. J. Lett. **951** (2023) [2306.16219].

[8] K.N. Ananda, C. Clarkson and D. Wands, *The Cosmological gravitational wave background from primordial density perturbations*, *Phys. Rev. D* **75** (2007) 123518 [gr-qc/0612013].

[9] D. Baumann, P.J. Steinhardt, K. Takahashi and K. Ichiki, *Gravitational Wave Spectrum Induced by Primordial Scalar Perturbations*, *Phys. Rev. D* **76** (2007) 084019 [hep-th/0703290].

[10] S. Mollerach, D. Harari and S. Matarrese, *CMB polarization from secondary vector and tensor modes*, *Phys. Rev. D* **69** (2004) 063002 [astro-ph/0310711].

[11] H. Assadullahi and D. Wands, *Constraints on primordial density perturbations from induced gravitational waves*, *Phys. Rev. D* **81** (2010) 023527 [0907.4073].

[12] J.R. Espinosa, D. Racco and A. Riotto, *A Cosmological Signature of the SM Higgs Instability: Gravitational Waves*, *JCAP* **09** (2018) 012 [1804.07732].

[13] K. Kohri and T. Terada, *Semianalytic calculation of gravitational wave spectrum nonlinearly induced from primordial curvature perturbations*, *Phys. Rev. D* **97** (2018) 123532 [1804.08577].

[14] NANOGrav collaboration, *The NANOGrav 12.5 yr Data Set: Search for an Isotropic Stochastic Gravitational-wave Background*, *Astrophys. J. Lett.* **905** (2020) L34 [2009.04496].

[15] V. De Luca, G. Franciolini and A. Riotto, *NANOGrav Data Hints at Primordial Black Holes as Dark Matter*, *Phys. Rev. Lett.* **126** (2021) 041303 [2009.08268].

[16] V. Vaskonen and H. Veermäe, *Did NANOGrav see a signal from primordial black hole formation?*, *Phys. Rev. Lett.* **126** (2021) 051303 [2009.07832].

[17] K. Kohri and T. Terada, *Solar-Mass Primordial Black Holes Explain NANOGrav Hint of Gravitational Waves*, *Phys. Lett. B* **813** (2021) 136040 [2009.11853].

[18] G. Domènech and S. Pi, *NANOGrav hints on planet-mass primordial black holes*, *Sci. China Phys. Mech. Astron.* **65** (2022) 230411 [2010.03976].

[19] V. Atal, A. Sanglas and N. Triantafyllou, *NANOGrav signal as mergers of Stupendously Large Primordial Black Holes*, *JCAP* **06** (2021) 022 [2012.14721].

[20] Z. Yi and Q. Fei, *Constraints on primordial curvature spectrum from primordial black holes and scalar-induced gravitational waves*, *Eur. Phys. J. C* **83** (2023) 82 [2210.03641].

[21] Z.-C. Zhao and S. Wang, *Bayesian Implications for the Primordial Black Holes from NANOGrav's Pulsar-Timing Data Using the Scalar-Induced Gravitational Waves*, *Universe* **9** (2023) 157 [2211.09450].

[22] V. Dandoy, V. Domcke and F. Rompineve, *Search for scalar induced gravitational waves in the International Pulsar Timing Array Data Release 2 and NANOgrav 12.5 years dataset*, 2302.07901.

[23] R.-G. Cai, C. Chen and C. Fu, *Primordial black holes and stochastic gravitational wave background from inflation with a noncanonical spectator field*, *Phys. Rev. D* **104** (2021) 083537 [2108.03422].

[24] K. Inomata, M. Kawasaki, K. Mukaida and T.T. Yanagida, *NANOGrav Results and LIGO-Virgo Primordial Black Holes in Axionlike Curvaton Models*, *Phys. Rev. Lett.* **126** (2021) 131301 [2011.01270].

[25] J. Garcia-Bellido, M. Peloso and C. Unal, *Gravitational Wave signatures of inflationary models from Primordial Black Hole Dark Matter*, *JCAP* **1709** (2017) 013 [1707.02441].

[26] G. Domènech and M. Sasaki, *Hamiltonian approach to second order gauge invariant cosmological perturbations*, *Phys. Rev. D* **97** (2018) 023521 [1709.09804].

[27] R.-g. Cai, S. Pi and M. Sasaki, *Gravitational Waves Induced by non-Gaussian Scalar Perturbations*, *Phys. Rev. Lett.* **122** (2019) 201101 [1810.11000].

[28] C. Unal, *Imprints of Primordial Non-Gaussianity on Gravitational Wave Spectrum*, *Phys. Rev. D* **99** (2019) 041301 [1811.09151].

[29] C. Yuan and Q.-G. Huang, *Gravitational waves induced by the local-type non-Gaussian curvature perturbations*, *Phys. Lett. B* **821** (2021) 136606 [2007.10686].

[30] V. Atal and G. Domènech, *Probing non-Gaussianities with the high frequency tail of induced gravitational waves*, *JCAP* **06** (2021) 001 [2103.01056].

[31] P. Adshead, K.D. Lozanov and Z.J. Weiner, *Non-Gaussianity and the induced gravitational wave background*, *JCAP* **10** (2021) 080 [2105.01659].

[32] H.V. Ragavendra, *Accounting for scalar non-Gaussianity in secondary gravitational waves*, *Phys. Rev. D* **105** (2022) 063533 [2108.04193].

[33] J.-P. Li, S. Wang, Z.-C. Zhao and K. Kohri, *Primordial Non-Gaussianity and Anisotropies in Gravitational Waves induced by Scalar Perturbations*, 2305.19950.

[34] S. Hawking, *Gravitationally collapsed objects of very low mass*, *Mon. Not. Roy. Astron. Soc.* **152** (1971) 75.

[35] E. Bugaev and P. Klimai, *Induced gravitational wave background and primordial black holes*, *Phys. Rev. D* **81** (2010) 023517 [0908.0664].

[36] R. Saito and J. Yokoyama, *Gravitational-Wave Constraints on the Abundance of Primordial Black Holes*, *Prog. Theor. Phys.* **123** (2010) 867 [0912.5317].

[37] S. Wang, T. Terada and K. Kohri, *Prospective constraints on the primordial black hole abundance from the stochastic gravitational-wave backgrounds produced by coalescing events and curvature perturbations*, *Phys. Rev. D* **99** (2019) 103531 [1903.05924].

[38] S.J. Kapadia, K. Lal Pandey, T. Suyama, S. Kandhasamy and P. Ajith, *Search for the Stochastic Gravitational-wave Background Induced by Primordial Curvature Perturbations in LIGO's Second Observing Run*, *Astrophys. J. Lett.* **910** (2021) L4 [2009.05514].

[39] A. Romero-Rodriguez, M. Martinez, O. Pujolàs, M. Sakellariadou and V. Vaskonen, *Search for a Scalar Induced Stochastic Gravitational Wave Background in the Third LIGO-Virgo Observing Run*, *Phys. Rev. Lett.* **128** (2022) 051301 [2107.11660].

[40] J.S. Bullock and J.R. Primack, *NonGaussian fluctuations and primordial black holes from inflation*, *Phys. Rev. D* **55** (1997) 7423 [astro-ph/9611106].

[41] C.T. Byrnes, E.J. Copeland and A.M. Green, *Primordial black holes as a tool for constraining non-Gaussianity*, *Phys. Rev. D* **86** (2012) 043512 [1206.4188].

[42] S. Young and C.T. Byrnes, *Primordial black holes in non-Gaussian regimes*, *JCAP* **08** (2013) 052 [1307.4995].

[43] G. Franciolini, A. Kehagias, S. Matarrese and A. Riotto, *Primordial Black Holes from Inflation and non-Gaussianity*, *JCAP* **03** (2018) 016 [1801.09415].

[44] S. Passaglia, W. Hu and H. Motohashi, *Primordial black holes and local non-Gaussianity in canonical inflation*, *Phys. Rev. D* **99** (2019) 043536 [1812.08243].

[45] V. Atal and C. Germani, *The role of non-gaussianities in Primordial Black Hole formation*, *Phys. Dark Univ.* **24** (2019) 100275 [1811.07857].

[46] V. Atal, J. Garriga and A. Marcos-Caballero, *Primordial black hole formation with non-Gaussian curvature perturbations*, *JCAP* **09** (2019) 073 [1905.13202].

[47] M. Taoso and A. Urbano, *Non-gaussianities for primordial black hole formation*, *JCAP* **08** (2021) 016 [2102.03610].

[48] D.-S. Meng, C. Yuan and Q.-g. Huang, *One-loop correction to the enhanced curvature perturbation with local-type non-Gaussianity for the formation of primordial black holes*, *Phys. Rev. D* **106** (2022) 063508 [2207.07668].

[49] C. Chen, A. Ghoshal, Z. Lalak, Y. Luo and A. Naskar, *Growth of curvature perturbations for PBH formation in non-minimal curvaton scenario revisited*, 2305.12325.

[50] R. Kawaguchi, T. Fujita and M. Sasaki, *Highly asymmetric probability distribution from a finite-width upward step during inflation*, 2305.18140.

[51] C. Fu, P. Wu and H. Yu, *Primordial black holes and oscillating gravitational waves in slow-roll and slow-climb inflation with an intermediate noninflationary phase*, *Phys. Rev. D* **102** (2020) 043527 [2006.03768].

[52] S. Young, C.T. Byrnes and M. Sasaki, *Calculating the mass fraction of primordial black holes*, *JCAP* **1407** (2014) 045 [1405.7023].

[53] G. Franciolini, A. Iovino, Junior., V. Vaskonen and H. Veermae, *The recent gravitational wave observation by pulsar timing arrays and primordial black holes: the importance of non-gaussianities*, 2306.17149.

[54] B. Carr, K. Kohri, Y. Sendouda and J. Yokoyama, *Constraints on primordial black holes*, *Rept. Prog. Phys.* **84** (2021) 116902 [2002.12778].

[55] N. Bartolo, D. Bertacca, V. De Luca, G. Franciolini, S. Matarrese, M. Peloso et al., *Gravitational wave anisotropies from primordial black holes*, *JCAP* **02** (2020) 028 [1909.12619].

[56] L. Valbusa Dall'Armi, A. Ricciardone, N. Bartolo, D. Bertacca and S. Matarrese, *Imprint of relativistic particles on the anisotropies of the stochastic gravitational-wave background*, *Phys. Rev. D* **103** (2021) 023522 [2007.01215].

[57] E. Dimastrogiovanni, M. Fasiello, A. Malhotra, P.D. Meerburg and G. Orlando, *Testing the early universe with anisotropies of the gravitational wave background*, *JCAP* **02** (2022) 040 [2109.03077].

[58] F. Schulze, L. Valbusa Dall'Armi, J. Lesgourgues, A. Ricciardone, N. Bartolo, D. Bertacca et al., *GW_CLASS: Cosmological Gravitational Wave Background in the Cosmic Linear Anisotropy Solving System*, 2305.01602.

[59] LISA Cosmology Working Group collaboration, *Probing anisotropies of the Stochastic Gravitational Wave Background with LISA*, *JCAP* **11** (2022) 009 [2201.08782].

[60] LISA Cosmology Working Group collaboration, *Cosmology with the Laser Interferometer Space Antenna*, 2204.05434.

[61] C. Ünal, E.D. Kovetz and S.P. Patil, *Multimessenger probes of inflationary fluctuations and primordial black holes*, *Phys. Rev. D* **103** (2021) 063519 [2008.11184].

[62] A. Malhotra, E. Dimastrogiovanni, M. Fasiello and M. Shiraishi, *Cross-correlations as a Diagnostic Tool for Primordial Gravitational Waves*, *JCAP* **03** (2021) 088 [2012.03498].

[63] M. Maggiore, *Gravitational wave experiments and early universe cosmology*, *Phys. Rept.* **331** (2000) 283 [gr-qc/9909001].

[64] S. Garcia-Saenz, L. Pinol, S. Renaux-Petel and D. Werth, *No-go theorem for scalar-trispectrum-induced gravitational waves*, *JCAP* **03** (2023) 057 [2207.14267].

[65] E. Komatsu and D.N. Spergel, *Acoustic signatures in the primary microwave background bispectrum*, *Phys. Rev. D* **63** (2001) 063002 [astro-ph/0005036].

[66] S. Pi and M. Sasaki, *Gravitational Waves Induced by Scalar Perturbations with a Lognormal Peak*, *JCAP* **09** (2020) 037 [2005.12306].

[67] E. Dimastrogiovanni, M. Fasiello, A. Malhotra and G. Tasinato, *Enhancing gravitational wave anisotropies with peaked scalar sources*, *JCAP* **01** (2023) 018 [2205.05644].

[68] G.P. Lepage, *Adaptive multidimensional integration: VEGAS enhanced*, *J. Comput. Phys.* **439** (2021) 110386 [2009.05112].

[69] Planck collaboration, *Planck 2018 results. VI. Cosmological parameters*, *Astron. Astrophys.* **641** (2020) A6 [1807.06209].

[70] K. Saikawa and S. Shirai, *Primordial gravitational waves, precisely: The role of thermodynamics in the Standard Model*, *JCAP* **1805** (2018) 035 [1803.01038].

[71] A.M. Green, A.R. Liddle, K.A. Malik and M. Sasaki, *A New calculation of the mass fraction of primordial black holes*, *Phys. Rev. D* **70** (2004) 041502 [astro-ph/0403181].

[72] T. Nakama, J. Silk and M. Kamionkowski, *Stochastic gravitational waves associated with the formation of primordial black holes*, *Phys. Rev. D* **95** (2017) 043511 [1612.06264].

[73] U. Seljak and M. Zaldarriaga, *A Line of sight integration approach to cosmic microwave background anisotropies*, *Astrophys. J.* **469** (1996) 437 [astro-ph/9603033].

[74] Y. Tada and S. Yokoyama, *Primordial black holes as biased tracers*, *Phys. Rev. D* **91** (2015) 123534 [1502.01124].

[75] C.R. Contaldi, *Anisotropies of Gravitational Wave Backgrounds: A Line Of Sight Approach*, *Phys. Lett. B* **771** (2017) 9 [1609.08168].

[76] N. Bartolo, D. Bertacca, S. Matarrese, M. Peloso, A. Ricciardone, A. Riotto et al., *Anisotropies and non-Gaussianity of the Cosmological Gravitational Wave Background*, *Phys. Rev. D* **100** (2019) 121501 [1908.00527].

[77] N. Bartolo, D. Bertacca, S. Matarrese, M. Peloso, A. Ricciardone, A. Riotto et al., *Characterizing the cosmological gravitational wave background: Anisotropies and non-Gaussianity*, *Phys. Rev. D* **102** (2020) 023527 [1912.09433].

[78] R.K. Sachs and A.M. Wolfe, *Perturbations of a cosmological model and angular variations of the microwave background*, *Astrophys. J.* **147** (1967) 73.

[79] M. Maggiore, *Gravitational Waves. Vol. 2: Astrophysics and Cosmology*, Oxford University Press (3, 2018).

[80] K. Schmitz, *New Sensitivity Curves for Gravitational-Wave Signals from Cosmological Phase Transitions*, *JHEP* **01** (2021) 097 [2002.04615].

[81] NANOGrav collaboration, *The NANOGrav 15-year Data Set: Search for Anisotropy in the Gravitational-Wave Background*, 2306.16221.